AD-A058 425 GRUMMAN AEROSPACE CORP BETHPAGE N Y RESEARCH DEPT F/G 20/4
THE VISCOUS TRANSONIC FLOW OVER TWO-ELEMENT AIRFOIL SYSTEMS.(U)
AUG 78 G VOLPE, B GROSSMAN N00014-75-C-0722
UNCLASSIFIED RE-558 ONR-CR215-241-2 NL

| OF |
ADA
058425

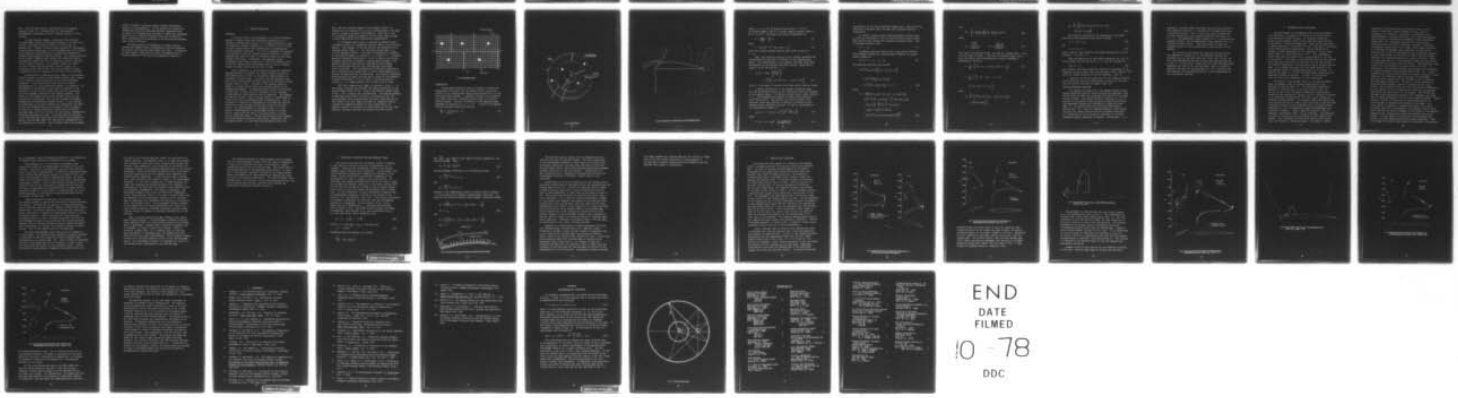

END
DATE
FILMED
10-78
DDC

LEVEL II

REPORT ONR-CR215-241-2

(12)

THE VISCOUS TRANSONIC FLOW OVER TWO-ELEMENT AIRFOIL SYSTEMS

G. VOLPE AND B. GROSSMAN

GRUMMAN AEROSPACE CORPORATION
RESEARCH DEPARTMENT
BETHPAGE, NEW YORK 11714

CONTRACT N00014-75-C-0722

1 AUGUST 1978

INTERIM REPORT FOR PERIOD 1 JANUARY 1977 – 30 SEPTEMBER 1977

PREPARED FOR THE

OFFICE OF NAVAL RESEARCH • 800 N. QUINCY ST. • ARLINGTON • VA • 22217

Change of Address

Organizations receiving reports on the initial distribution list should confirm correct address. This list is located at the end of the report. Any change of address or distribution should be conveyed to the Office of Naval Research, Code 211, Arlington, VA 22217.

Disposition

When this report is no longer needed, it may be transmitted to other organizations. Do not return it to the originator or the monitoring office.

Disclaimer

The findings and conclusions contained in this report are not to be construed as an official Department of Defense or Military Department position unless so designated by other official documents.

Reproduction

UNCLASSIFIED

SECURITY CLASSIFICATION OF THIS PAGE (When Data Entered)

REPORT DOCUMENTATION PAGE	READ INSTRUCTIONS BEFORE COMPLETING FORM
1. REPORT NUMBER: ONR-CR215-241-2	2. GOVT ACCESSION NO.
3. RECIPIENT'S CATALOG NUMBER	
4. TITLE (and Subtitle): The Viscous Transonic Flow over Two-Element Airfoil Systems.	5. TYPE OF REPORT & PERIOD COVERED: Interim Report, 1 Jan [illegible] - 30 Sep [illegible] 77
6. PERFORMING ORG. REPORT NUMBER: RE-558	
7. AUTHOR(s): G. Volpe, B. Grossman	8. CONTRACT OR GRANT NUMBER(s): N00014-75-C-0722
9. PERFORMING ORGANIZATION NAME AND ADDRESS: Grumman Aerospace Corporation, Bethpage, New York 11714	10. PROGRAM ELEMENT, PROJECT, TASK AREA & WORK UNIT NUMBERS
11. CONTROLLING OFFICE NAME AND ADDRESS: Office of Naval Research, 800 N. Quincy Street, Arlington, Virginia 22217	12. REPORT DATE: Aug [illegible] 78
	13. NUMBER OF PAGES: 49 p.
14. MONITORING AGENCY NAME & ADDRESS (if different from Controlling Office)	15. SECURITY CLASS. (of this report): UNC.
	15a. DECLASSIFICATION/DOWNGRADING SCHEDULE

16. DISTRIBUTION STATEMENT (of this Report)

Approved for public release; distribution unlimited.

17. DISTRIBUTION STATEMENT (of the abstract entered in Block 20, if different from Report)

18. SUPPLEMENTARY NOTES

19. KEY WORDS (Continue on reverse side if necessary and identify by block number)

Transonic Flow, Two-Element Airfoil Systems, Slats, Flaps, Viscous Flow

20. ABSTRACT (Continue on reverse side if necessary and identify by block number)

A numerical procedure has been developed to compute the transonic viscous-inviscid interacting flow field about airfoils with leading edge slats or trailing edge flaps. The inviscid theory utilizes conformal mappings in a full potential flow formulation, with analytic removal of singularities and a mixed flow relaxation procedure. The turbulent boundary layer is computed with methods based on a turbulent kinetic energy formulation and is coupled to the inviscid flow using surface source flow boundary conditions.

next page

DD FORM 1 JAN 73 1473 EDITION OF 1 NOV 65 IS OBSOLETE

S/N 0102-014-6601

406 165

UNCLASSIFIED

SECURITY CLASSIFICATION OF THIS PAGE (When Data Entered)

Semiempirical methods are used to compute local strong interaction regions occurring in the vicinity of shock waves, trailing edges, and to account for flow separation. Our results are in good agreement with existing wind tunnel data for several typical two-element airfoil configurations.

Report ONR-CR-215-241-2
RE-558

THE VISCOUS TRANSONIC FLOW OVER TWO-ELEMENT AIRFOIL SYSTEMS

Interim Report for Period 1 January 1977 - 30 September 1977

by

G. Volpe and B. Grossman

Prepared Under Contract N00014-75-C-0722

for

Office of Naval Research
800 N. Quincy St.
Arlington, VA 22217

by

Research Department
Grumman Aerospace Corporation
Bethpage, New York 11714

August 1978

Approved by: Richard A. Scheuing
Richard A. Scheuing
Director of Research

ABSTRACT

A numerical procedure has been developed to compute the transonic viscous-inviscid interacting flow field about airfoils with leading edge slats or trailing edge flaps. The inviscid theory utilizes conformal mappings in a full potential flow formulation, with analytic removal of singularities and a mixed flow relaxation procedure. The turbulent boundary layer is computed with methods based on a turbulent kinetic energy formulation and is coupled to the inviscid flow using surface source flow boundary conditions. Semiempirical methods are used to compute local strong interaction regions occurring in the vicinity of shock waves, trailing edges, and to account for flow separation. Our results are in good agreement with existing wind tunnel data for several typical two-element airfoil configurations.

TABLE OF CONTENTS

LIST OF ILLUSTRATIONS

LIST OF SYMBOLS

a	local speed of sound
C_L	lift coefficient
E_1	defined by Eq. (11)
E_2	defined by Eq. (11)
f	defined by Eq. (3)
G	reduced potential
H	metric of conformal mappings
$\tilde{H}$	reduced metric
k, k_1, k_2	mapping constants
L	defined by Eq. (9b)
M	Mach number
Re	Reynolds number
r	radial direction in annular domain
r_s	radius of inner ring corresponding to secondary airfoil in annular domain
r_∞	radius of point of infinity in annular domain
U	velocity component parallel to surface
u	velocity component in r direction
u_1	defined by Eq. (15)
V	velocity component normal to surface
V_s	surface source distribution
v	velocity component in θ direction
v_1	defined by Eq. (14)
x	local streamwise coordinate
y	local coordinate normal to streamlines
x, y	cartesian coordinates in physical plane

Z	complex annular domain, $= re^{i\theta}$
α	angle of attack
β	defined by Eq. (6)
γ	ratio of specific heats
Γ_1, Γ_2	circulation constants for main and secondary airfoils
δ^*	displacement thickness
θ	azimuthal direction in annular domain
Φ	complete potential function
Φ_1	free stream condtribution to potential
Φ_2	circulatory flow contribution to potential
Φ_3	additional circulatory flow contribution to potential
ρ	density
ψ	stream function

Subscripts

o	value at airfoil surface
e	value at edge of boundary layer
∞	free stream quantity

1. INTRODUCTION

For an aircraft to maneuver effectively in the transonic speed range, its wing must generate high lift coefficients without incurring excessive drag or buffet. The recent development of supercritical wings can enable a designer to meet this specification. However this requirement will often degrade the aircraft's performance at cruise with larger than optimal drag coefficients. The implementation of high-lift devices at transonic speeds offers the possibility of greatly enhancing the maneuvering capabilities of modern aircraft without compromising their cruising efficiency. This possibility has been proven in the last few years by the installation of slats on the F-4 and the positive test of a slatted wing on the F-14 aircraft. The performance of these aircraft in managing climbs and turns at transonic speeds was remarkably improved by the presence of the slats, even though these configurations have not been shown to be optimal by any means.

The aerodynamic designer currently lacks an analytical tool to design, or even analyze, transonic airfoils with high-lift devices. Furthermore the paucity of experimental data currently makes it difficult to determine what can be achieved with these maneuvering devices. Also, accumulating experimental data on such configurations would be extremely expensive in light of the number of configurations that need be tested and the high speeds and Reynolds numbers required in a meaningful wind-tunnel test program. A theoretical tool for the analysis of the transonic flow over two-element airfoil systems would be a valuable first step in aiding the designer by reducing the number of configurations that need be tested and by providing insight into the flow phenomena that are present at high speeds.

This report describes the development of a method for numerically computing the viscous transonic flow over an airfoil with a leading-edge slat or a trailing-edge flap.

Practical designs will primarily require slat configurations, but since the method is applicable to general two-element airfoil systems, both slats and flaps are considered. In general, even the inviscid flow fields on these configurations are difficult to obtain analytically because of the complicated geometry of the multiply-connected domain. Small-disturbance approximations (such as that used for this problem in Ref. 1) do not appear to be adequate since the interaction of the flow between the airfoils will provide large perturbations to the flow field.

In recent years the application of mixed-flow relaxation techniques, introduced by Murman and Cole (Ref. 2) has made possible the numerical computation of inviscid transonic flows over a variety of geometrical shapes in both two and three dimensions. These methods are generally based on the assumption of irrotational flow and solve either the full potential equation or an appropriate form of the small-disturbance equations. For two-dimensional flows in particular, accurate and efficient solutions to the full potential equation have been obtained for transonic flows over airfoil sections (Refs. 3 and 4) over axisymmetric bodies (Refs. 5 and 6) and over nacelles (Refs. 7 and 8).

More recently, as reported in Refs. 9 and 10, these relaxation techniques have been applied to compute the flow about an airfoil with a slat or a flap at transonic speeds. The approach as discussed in Ref. 10 and summarized in Section 2 is to solve the full inviscid, irrotational flow equations about two-element airfoil systems. The methodology consists of the 1) development of a suitable computational plane and grid system, 2) evaluation of an appropriate set of governing inviscid equations and boundary conditions in terms of smoothly-varying, single-valued functions in the computational domain, and 3) establishment of a stable and accurate numerical procedure for the solution of the governing equations. An abbreviated version of the inviscid analysis appears in

Ref. 9 with further details, particularly on the mapping methods in Ref. 10. Arlinger (Ref. 11) has recently independently developed a similar inviscid analysis of this problem.

At high Reynolds numbers, solutions of the inviscid flow equations provide a reasonable estimate of the lift on an airfoil, provided the angle of attack is below that for maximum lift. However, inviscid theory provides no information on skin friction, form drag, or on the maximum lift of an airfoil. These important characteristics are completely dominated by boundary layer growth on airfoil surfaces. For standard airfoils at low speeds, boundary layer effects are relatively weak at high Reynolds number and can be treated as a small correction to the inviscid solution. At transonic speeds, for supercritical airfoils and multielement airfoil systems, the situation is much more severe, with viscous effects playing a significant role in reducing the lift from inviscid values.

Our approach to computing viscous effects on two-element airfoil systems is based on second-order boundary layer theory with a surface source formulation of the viscous matching conditions. The inviscid and viscous flows are solved simultaneously in a self-consistent fashion, by iteration. The development of the boundary layer over the surfaces of the airfoils is driven by the inviscid flow with the equivalent mass flow boundary condition on the airfoil surfaces. The effect of the boundary layer on the inviscid flow, and the circulation in particular, will be felt through the renewed computation with equivalent surface sources. In our analysis we assume that the airfoil elements are sufficiently far apart so that the boundary layers do not merge in the slot region. To account for strong interaction regions near the airfoil trailing edges and in the vicinity of shock waves, semiempirical smoothing procedures are used. A rational analytic approach to the trailing edge interaction has recently been proposed by Melnik, Chow and Mead (Ref. 12), and will be implemented into our approach in the future. Most available data on two-element

airfoil systems at transonic speeds indicate substantial regions of flow separation. In the absence of a definitive theoretical method for treating turbulent separated flows, we resort to a semiempirical procedure to model this phenomena. Details of our viscous flow method are given in Section 3, with a discussion of the coupling of the inviscid and boundary layer flows in Section 4.

We have applied our computation to several typical slatted and flapped airfoil configurations and have compared our results with existing wind tunnel test data. A discussion of these results along with our future recommendations of further research in this area are presented in Section 5.

2. INVISCID SOLUTION

MAPPINGS

A crucial step in the development of a finite-difference method to compute flows over complicated geometries is to develop a suitable grid system. It is highly desirable to have the geometric contours aligned with a coordinate line in order to avoid interpolations and extrapolations in applying the surface boundary conditions. It is also convenient for external flow problems to map the infinite physical domain to a finite computational space in order to accurately apply the far-field boundary conditions. Furthermore, the mappings should concentrate grid lines in regions of steep flow gradients such as airfoil leading and trailing edges and in the slot formed between the main airfoil and the slat or flap.

In our approach, we use analytic and numerical conformal mapping methods to transform the infinite domain external to two-element airfoil system to the annular region between two concentric circular rings. The outer ring corresponds to the main airfoil surface and the inner ring to the secondary airfoil surface (flap or slat). Infinity in the physical plane is mapped to a single point within the circular annulus in the computational domain. The mapping method follows from the work of Ives (Ref. 13) and utilizes a sequence of five conformal transformations, three analytic and two numerical. The mapping proceeds as follows: First the main airfoil is transformed to a near circle by a Von Karman-Trefftz transformation. This is followed by a Theodorsen transformation utilizing fast-Fourier transforms to map the main airfoil near circle to an exact circle. The third mapping, as outlined in Ref. 13, is an analytic transformation of the secondary airfoil to a near circle, which keeps the image of the main airfoil a circle (but of different radius). (In the application of this mapping, we have developed an approach which greatly simplifies some procedures in Ref. 13, and these are discussed in Ref. 10.)

Next, the near circular image of the secondary airfoil is centered at the interior of the circle corresponding to the main airfoil through a bilinear transformation. And finally, the two concentric shapes are mapped to two circular rings through a second application of the Theodorsen transformation.

An orthogonal grid system is produced by taking a polar-coordinate system (r,θ) emanating from the center of the circular annulus. The surfaces of the two airfoils are obtained as two constant radius lines, $r = 1$ for the main airfoil and $r = r_s$ for the secondary airfoil. The point corresponding to infinity in the physical domain is located at $r = r_\infty$ and $\theta = 0$. A further analytic coordinate stretching $X = X(\theta)$ is used in the circumferential direction to produce a suitable grid spacing in the physical plane with mesh points concentrated near leading and trailing edges and with each trailing edge coinciding with a grid point. The circumferential stretching discussed in Ref. 10 required the program user to select three parameters to achieve the desired point concentration. An alternate stretching which requires no inputs from the user is given in the Appendix. A radial stretching $Y = Y(r)$ is used to locate the point of infinity, $r = r_\infty$, midway between the circular airfoil rings.

The final computational domain is sketched in Fig. 1. In this plane a uniform grid produces the mesh distribution in the annular domain shown in Fig. 2 and in the physical domain shown in Fig. 3 for a typical slat configuration. The mapping produces a grid where each airfoil surface is a coordinate line, the trailing edges occur on mesh points and with a high density of grid lines in the slot region and near all stagnation points. Although the mapping procedure is quite complicated, our computer program to calculate the coefficients of all the terms generally requires less than 10 seconds on an IBM 370/168.

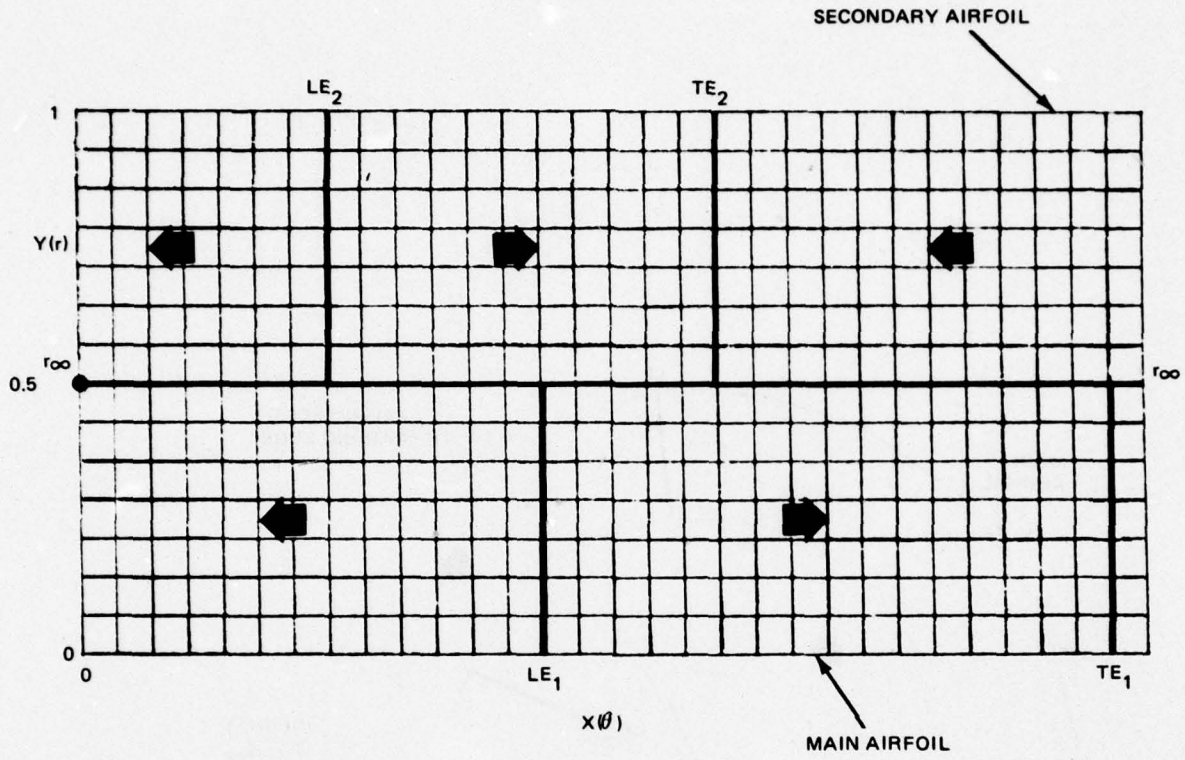

Fig. 1 Computational Domain

FORMULATION

The governing equations for the inviscid, irrotational compressible flow about the two-element airfoil system are written in the computational domain using the metric H, of the above-mentioned mappings. A potential function is introduced into these equations. Singularities are seen to arise for several reasons. Firstly, the metric of the mapping becomes unbounded at infinity ($r = r_\infty$, $\theta = 0$). A study of the mapping function indicates that near infinity

$$\frac{d\zeta}{dZ} \to \frac{k}{(Z-r_\infty)^2} \text{ as } Z \to r_\infty \qquad (1)$$

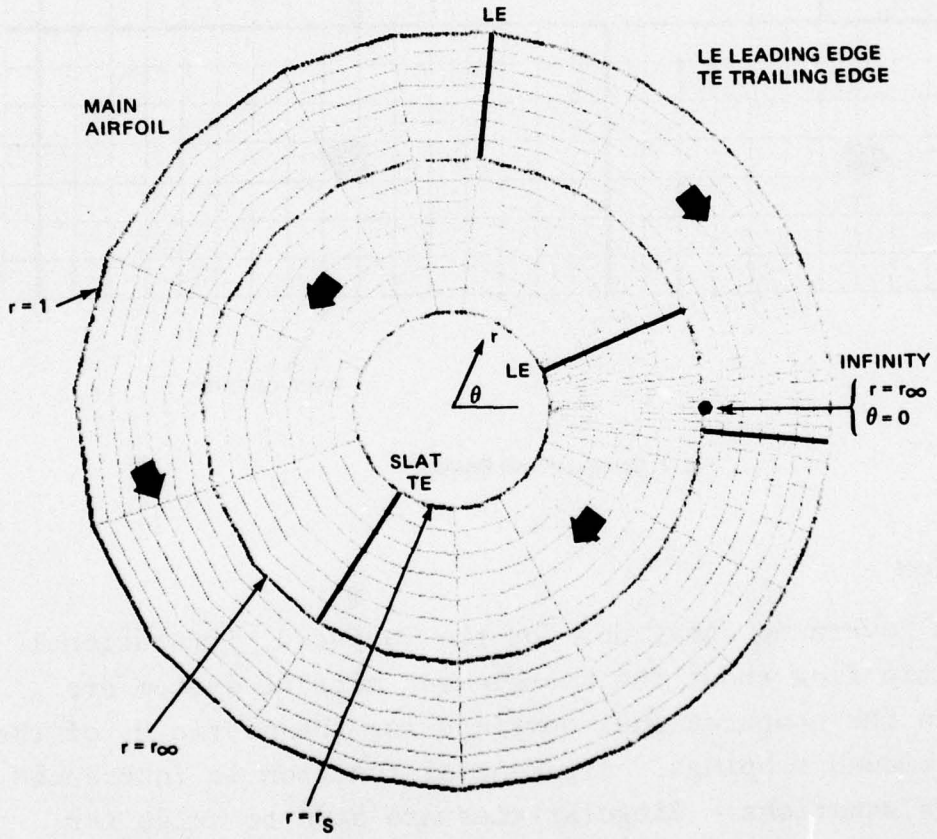

Fig. 2 Annular Domain

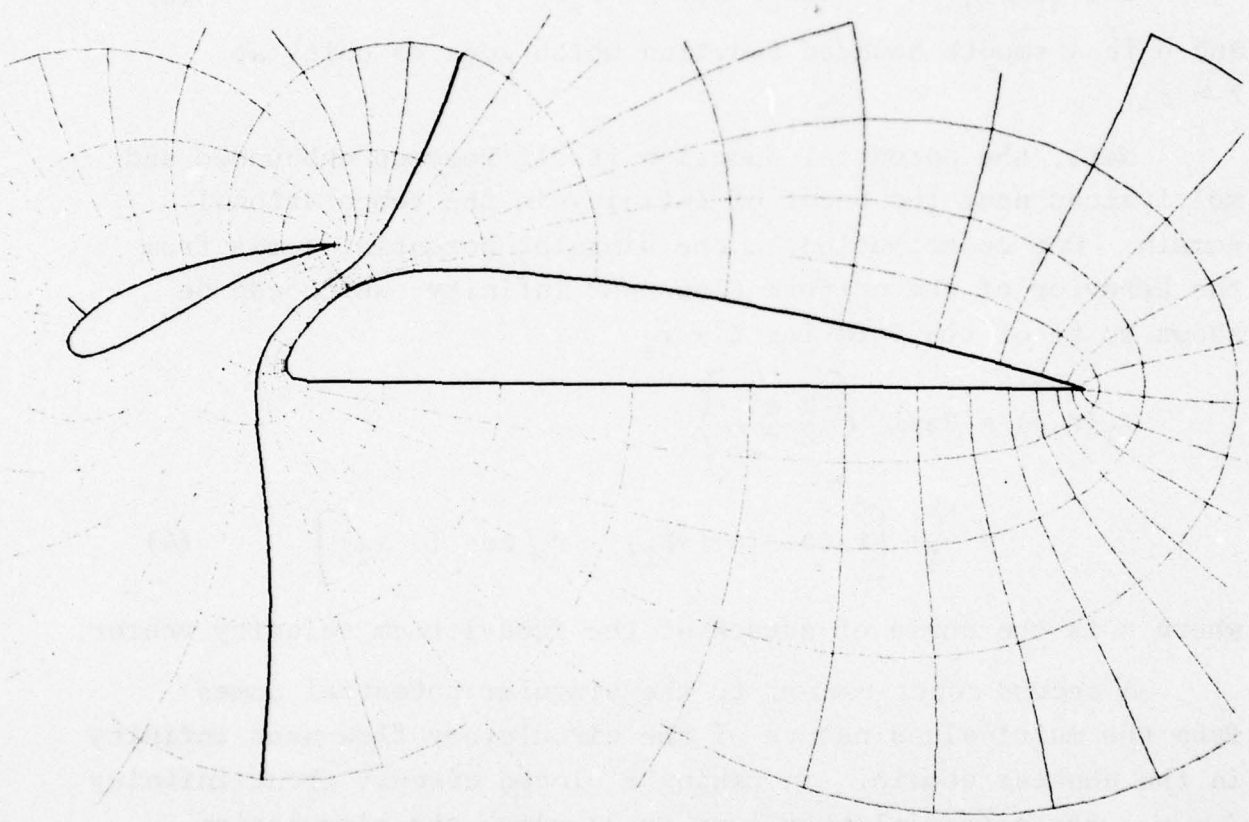

Fig. 3 Coordinate Grid – Physical Plane Clark Y Airfoil/30% Maxwell Slat

where $\zeta = x + iy$ in the physical plane and $Z = r\, e^{i\theta}$ in the annular domain, and k is a known complex constant taken to be $k = k_1\, e^{ik_2}$. The metric may then be regularized by

$$H = \left|\frac{d\zeta}{dZ}\right| = \frac{k_1}{f}\,\tilde{H} \tag{2}$$

where

$$f \equiv \left|Z - r_\infty\right|^2 = r^2 - 2r_\infty r\cos\theta + r_\infty^2 \tag{3}$$

and $\tilde{H}$ is a smooth bounded function which goes to unity at $Z = r_\infty$.

Next, the potential function itself becomes unbounded and multivalued near the point of infinity in the computational domain. One contribution to the singular potential comes from the behavior of the uniform flow near infinity, which can be shown to be of the form for $Z \to r_\infty$

$$\phi_1(r,\theta) = \text{Real}\left\{\frac{-k\, e^{i\alpha}}{Z - r_\infty}\right\}$$

$$= \frac{-k_1}{f}\left[r\cos\left(\theta + \alpha - k_2\right) - r_\infty\cos\left(\alpha - k_2\right)\right] \tag{4}$$

where α is the angle of attack of the free-stream velocity vector.

A second contribution to the singular potential comes from the multivalued nature of the circulatory flow near infinity in the annular domain. In taking a closed circuit about infinity $Z = r_\infty$, the potential must jump by 2π times the circulation about each airfoil. The solution for the circulatory flow potential valid near infinity is found as a solution to the Prandtl-Glauert equations (see Ref. 14) and is transformed to the computational domain as

$$\phi_2(r,\theta) = -\left(\Gamma_1 + \Gamma_2\right)\tan^{-1}\left[\sqrt{1 - M^2}\tan\beta\right] \tag{5}$$

where

$$\beta = k_2 - \alpha + \pi - \tan^{-1}\left(\frac{r\sin\theta}{r\cos\theta - r_\infty}\right) \tag{6}$$

and where M_∞ is the free-stream Mach number and Γ_1 and Γ_2 are the circulation constants about the main and secondary airfoils, respectively.

To obtain a single-valued reduced potential another term, ϕ_3, must be introduced so that any closed contours about individual airfoils will produce the required circulation jump. This is obtained through a term

$$\phi_3 = - \Gamma_2 \theta \tag{7}$$

A reduced potential function $G(r,\theta)$ may now be defined which remains bounded and single-valued throughout the entire annular domain as

$$G(r,\theta) = \Phi - \Phi_1 - \Phi_2 - \Phi_3 \tag{8}$$

The governing equations then become

$$(a^2-v^2) f G_{rr} - 2uvf \left[\frac{1}{r} G_{r\theta} - \frac{1}{r^2} (G_\theta - \Gamma_2) \right]$$

$$+ (a^2-u^2) f \left(\frac{1}{r^2} G_{\theta\theta} + \frac{1}{r} G_r \right)$$

$$+ (u^2+v^2) k_1 \left(v\tilde{H}_r + \frac{u}{r} \tilde{H}_\theta \right) + L = 0 \tag{9a}$$

where

$$L \equiv - \frac{4uv}{r} \left[(r - r_\infty \cos\theta) (G_\theta - \Gamma_2) + r_\infty r \sin\theta \, G_r \right]$$

$$+ 2(u^2-v^2) \left[(r - r_\infty \cos\theta) G_r - \frac{r_\infty}{r} \sin\theta (G_\theta - \Gamma_2) \right]$$

$$- (\Gamma_1+\Gamma_2) \frac{E_1}{f} \left\{ 2(u^2-v^2) (r - r_\infty \cos\theta) \right.$$

$$r_\infty \sin\theta + 2uv(f - 2r_\infty^2 \sin^2\theta)$$

$$\left. - E_2 \left[a^2 f - (v r_\infty \sin\theta - ur + ur_\infty \cos\theta)^2 \right] \right\} \tag{9b}$$

and

$$a^2 = \left[1+\left(\frac{\gamma-1}{2}\right) M_\infty^2\right] / M_\infty^2 - \left(\frac{\gamma-1}{2}\right)(u^2+v^2) \tag{10}$$

where

$$E_1 \equiv \frac{\sqrt{1-M_\infty^2}}{1-M_\infty^2 \sin^2\beta} \quad , \qquad E_2 \equiv \frac{-M_\infty^2 \sin 2\beta}{1-M_\infty^2 \sin^2\beta} \tag{11}$$

and f and β are defined in Eqs. (3) and (6), respectively. Also, a is the speed of sound, γ the ratio of specific heats, and v and u the radial and circumferential velocity components, respectively, given by

$$v = \frac{1}{Hk_1}\left\{ fG_r - (\Gamma_1 + \Gamma_2) E_1 r_\infty \sin\theta + v_1 \right\} \tag{12}$$

$$u = \frac{1}{Hk_1}\left\{ \frac{f}{r}(G_\theta - \Gamma_2) - (\Gamma_1 + \Gamma_2) E_1 (r_\infty \cos\theta - r) + u_1 \right\} \tag{13}$$

where

$$v_1 \equiv \frac{k_1}{f}\left[r^2 \cos(\theta+\alpha-k_2) - 2r_\infty r \cos(\alpha-k_2) + r_\infty^2 \cos(\theta-\alpha+k_2)\right] \tag{14}$$

$$u_1 \equiv \frac{k_1}{f}\left[r^2\sin(\theta+\alpha-k_2)-2r_\infty r\sin(\alpha-k_2)\right.$$
$$\left.-r_\infty^2\sin(\theta-\alpha+k_2)\right] \qquad (15)$$

The boundary condition of the vanishing of the normal velocity on the surface of each airfoil becomes

$$v = 0 \quad \text{on } r = r_s \qquad (16)$$

and

$$v = 0 \quad \text{on } r = 1 \qquad (17)$$

which, from Eq. (12) specifies the normal derivative G_r on the surfaces $r = r_s$ and $r = 1$.

With the definition of the reduced potential, Eq. (8), it can be shown that the solution at $Z = r_\infty$ may be specified as

$$G(r_\infty, 0) = 0 \qquad (18)$$

And, finally, the Kutta condition requires the vanishing of the tangential velocity $\tilde{u}_H$ at each trailing edge, which, from Eq. (13) gives two linear equations in the two unknowns Γ_1 and Γ_2.

A good set of initial conditions for the reduced potential can be obtained from the incompressible solution for the flow over two circles developed by Lagally (Ref. 15).

FINITE-DIFFERENCE PROCEDURE

The numerical formulation of the Neumann boundary-value problem described above for mixed subsonic and supersonic flow follows from the ideas and techniques developed for the single airfoil problem. The reduced potential equation, Eq. (9) is solved by a successive column relaxation algorithm utilizing type-dependent differencing originated by Murman and Cole (Ref. 2). Our method stems from techniques developed by Jameson (Ref. 16). Since our mapping produces a grid system that does not remain aligned with the streamwise direction, it is necessary to use a coordinate invariant or "rotated" difference scheme, developed by Jameson. Furthermore, it is

necessary to develop sweep directions that are less than 90^{o} to the streamline direction. A suitable set of sweep directions, illustrated in Figs. 1 and 2, consists of first dividing the circular annulus into two sections divided by the ring $r = r_{\infty}$ or $Y = \frac{1}{2}$. Circumferential lines interior to $r = r_{\infty}$ surround the secondary airfoil, and circumferential lines exterior to $r = r_{\infty}$ surround the main airfoil. Sweep directions are from the stagnation point to the trailing edge of each airfoil in the annulus.

At the end of each sweep new values of the circulation are computed by setting $\tilde{u}_H = 0$, and therefore setting the bracketed term on the right hand side of Eq. (13) to zero, at each trailing edge and solving the two resulting equations for Γ_1 and Γ_2. In some cases, where there are large circumferential gradients near one of the trailing edges, such as a shock or expansion fan near the trailing edge of a slat, stability has been enhanced through underrelaxation of the determination of the circulation constants.

3. BOUNDARY LAYER CALCULATION

The development of the boundary layer over the surfaces of the airfoils is assumed to be driven by the inviscid flow with equivalent surface sources. At transonic speeds the growth of the boundary layers on the upper and lower surfaces of an airfoil is highly unsymmetrical. High aft-loadings cause a rapid thickening in the airfoil top and a thinning on the bottom as the trailing edge is approached. The net effects is to produce a strong uncambering of the "equivalent" airfoil shape which leads to a sharp reduction in lift. This uncambering effect could also be looked at as a strong upwash at the rear of the airfoil. The effect of the boundary layer on the inviscid flow, and the circulation in particular, will be felt through the renewed computation of the equivalent source strength on the body. It is assumed that gap sizes are large enough so that the boundary layers of neighboring surfaces do not merge. In addition the effect of a finite thickness wake passing over the downstream element is ignored. In light of the practical sizes of slats these assumptions are not significant.

The growth of the boundary layer in its initial laminar stage is computed using an integral method based on the approach of Thwaites (Ref. 17). The particular formulation employed is that described by Rott and Crabtree (Ref. 18) who by the use of the Illingworth-Stewartson transformation showed how the compressible laminar flow on a surface is reduced to an equivalent incompressible flow that can be computed by Thwaites' original method. At transonic speeds the laminar run on an airfoil surface is usually quite short and it was felt that sufficient accuracy would be obtained with an integral method. Transition is still an imperfectly understood phenomenon and difficult to predict. Several empirical criteria, such as Crabtree's and Michel's (Ref. 19) are available. Alternatively, the point of transition can be specified in the computational method. Since transition is most often fixed in wind tunnel test this feature is extremely useful. In addition, should

separation be predicted while the boundary layer is still laminar, transition is again assumed to occur, and the computation is continued. Transition is assumed to occur instantaneously, and from this point on the turbulent boundary layer solution is obtained with Bradshaw's finite difference method (Ref. 20). Starting conditions for the turbulent calculation are obtained by requiring continuity of the mass and momentum fluxes within the boundary layer during transiton. In the method of Bradshaw three equations, the mean motion equations for continuity and momentum and an empirical equation for the shear stress obtained from the exact turbulent energy equation, are integrated numerically along the surface. Since the three equations are of an hyperbolic nature the integration is performed by marching along the surface. This method has been shown to be very accurate for a wide variety of flows. Alternatively, the turbulent boundary layer growth can be computed by Green's integral lag-entrainment method (Ref. 21). Green's method solves at each station along the surface a system of three equations, the momentum integral equation, an entrainment equation and an equation for the streamwise rate of change of the entrainment coefficient. The last of these equations was developed from Bradshaw's empirical equation for the shear stress. The two methods have thus the same physical foundations, and the results of the two methods agree very well and produce essentially the same results in the program. Both methods are included in the program now because of the advantages each might have in future developments of the viscous analysis method. Green's method is capable of continuing the calculation beyond the trailing edge to determine the thickness of the wake. At a later time it is planned to examine the effects of a finite thickness wake and of the merging of the boundary layers and/or wakes from the two airfoil elements on the results of the program especially for configurations where the elements are closely spaced. In cases where the interaction of the merging shear layers is strong integral methods may become inaccurate. Thus, even though at present Green's method is sufficient, the possible

use of Bradshaw's finite difference procedure in the computation of merging flows justifies its presence in the program.

The parameters of interest which the boundary layer computation yields are the displacement thickness and the skin friction. The latter is integrated to give the skin friction drag on the airfoil configuraton. Following the approaches taken in the theoretical methods of analysis for single-airfoil transonic flows and multi-element incompressible flows, the major effect of the boundary layer on the inviscid flow is through weak displacement effects. Within these theories correction to the inviscid solution can be obtained by determining the inviscid flow over an equivalent body obtained either by adding the displacement thickness to the airfoil, or alternatively, as in the present approach, by allowing for an appropriate mass flow at the airfoil surface (Ref. 22).

These procedures are uniformly valid in regions where the surface geometry is smooth and the inviscid surface pressures are regular. Unfortunately in regions of strong interactions, such as trailing edges and shocks, ordinary boundary layer theory breaks down. In the past empirical corrections have been used quite successfully to compute the displacement effects in strong interaction regions. Since the purpose of constructing an equivalent body is to have a surface around which the flow can be considered inviscid, a way to account for strong interaction regions, short of actually building accurate theoretical models and solving them, is to model the inviscid streamline in these regions. This is the approach that is followed here.

The shock wave-boundary layer interaction has somewhat of a local nature. The boundary layer spreads the pressure gradient of the shock in the free stream over several boundary layer thicknesses on the surface (Ref. 23). Often a bubble of separated flow will occur under the foot of the shock. In such a case, the flow around the airfoil is only affected locally. Only if the shock is strong enough to separate the boundary layer will

the flow at the trailing edge and, hence, the circulation be greatly affected. The approach, thus, is to smear the pressure rise through the shock over a short distance and continue the boundary layer computation still accepting the calculated displacement thickness as an adequate representation of the inviscid streamline. Often the inviscid calculation itself will smooth the shock sufficiently for the boundary layer computation to proceed without separating. A steep pressure rise is spread over a short distance will produce a "bump" in the displacement thickness. As the rise is spread over a larger distance this "bump" will decrease and enough smoothing will eliminate it. Downstream of the shock wave the boundary layer characteristics are remarkably independent of the degree of smoothing. The downstream boundary layer growth is practically independent of the shock modeling; and it is the rate of growth rather than the magnitude of the displacement thickness as the trailing edge is approached that determines the decrease in circulation due to the boundary layer. The displacement surface obtained in this manner near the shock approximates very closely the "bump" model proposed by Yoshihara and Murman (private communication) without a tendency to introduce instabilities in the solution.

Near a trailing edge second-order boundary layer theory again becomes singular. The displacement thickness slope and hence equivalent mass flow grows without bound as the trailing edge is approached. Boundary layer calculation programs such as Bradshaw's or Green's reflect this feature. There is extensive evidence (Ref. 12) to indicate that the trailing edge singularity is eliminated when the boundary layer and inviscid flow are solved simultaneously, in an iterative fashion. However due to possible numerical errors in the trailing edge region, the displacement thickness is smoothed on a scale of a few boundary layer thicknesses at the trailing edge.

The approach followed in single-element airfoil programs such as those described in Refs. 24-26 has been to extrapolate δ^* from a short distance upstream, thus providing a smooth streamline passing over the trailing edge. This method gives a good representation of the equivalent body locally. As such, this is the approach currently followed in the present method. Recent developments will make available an approach that does not rely on this kind of empiricism. The work of Melnik, Chow and Mead (Ref. 12) provides a closed form representation for the local trailing edge solution, and this would replace the extrapolation procedure currently relied on.

4. COUPLING OF INVISCID FLOW AND BOUNDARY LAYER

The viscous flow over the two-element system is computed in the form of an inviscid flow over an equivalent set of surfaces. These are the streamlines closest to the airfoil elements where viscosity can be neglected. The equivalent body can be obtained by numerically changing the ordinates of the airfoil system, which would necessitate a remapping of the configuration in order to compute a new inviscid flow. An equivalent and simpler procedure which avoids the need to remap is to change the boundary condition at the airfoil surface from one of zero flow through the surface to one of nonzero normal velocity with a value wich makes the equivalent body a streamline. In this formulation a source distribution computed from the displacement thickness is placed at the surface of the airfoils (i.e. see Lighthill (Ref. 22)). This source distribution is obtained by enforcing the condition that the displacement surface be a streamline. In the notation of Fig. 4 this means that the streamfunction, ψ_e, defining the equivalent body is equal to zero. The nearby airfoil surface (no longer a streamline), here denoted by ψ_0, can be developed from ψ_e by a one term Taylor series expansion; thus

$$\psi_0 = \psi_e - y_e \frac{\partial \psi}{\partial y} = - y_e \frac{\partial \psi}{\partial y} \tag{19}$$

Since $y_e = \delta^*$ and $\frac{\partial \psi}{\partial y} = +\rho_e U_e$, it follows that

$$\psi_0 = - \rho_e U_e \delta^* \tag{20}$$

Differentiating with respect to x yields

$$\frac{\partial \psi_0}{\partial x} = - \frac{\partial}{\partial x} (\rho_e U_e \delta^*)$$

Now, $\frac{\partial \psi_0}{\partial x} = -\rho_e V_s$, where V_s the normal velocity component at the airfoil surface. Thus,

$$V_s = \frac{1}{\rho} \frac{\partial}{\partial x} (\rho_e U_e \delta^*) \tag{21}$$

The new boundary conditions to be satisfied are then

$$\phi_r = \frac{\tilde{Hk}_1}{f} V_s, \text{ on } r = r_s \tag{22}$$

and

$$\phi_r = \frac{\tilde{Hk}_1}{f} V_s, \text{ on } r = 1$$

because in the computational plane a positive source strength is in the direction of negative computational velocities. In terms of the reduced potential these boundary conditions become

$$G_r = \frac{1}{f} \left[\tilde{Hk}_1 V_s + (\Gamma_1 + \Gamma_2) E_1 r_\infty \sin \theta - v_1 \right]$$

$$\text{on } r = r_s \tag{23}$$

and

$$G_r = \frac{1}{f} \left[-\tilde{Hk}_1 V_s + (\Gamma_1 + \Gamma_2) E_1 r_\infty \sin \theta - v_1 \right]$$

$$\text{on } r = 1$$

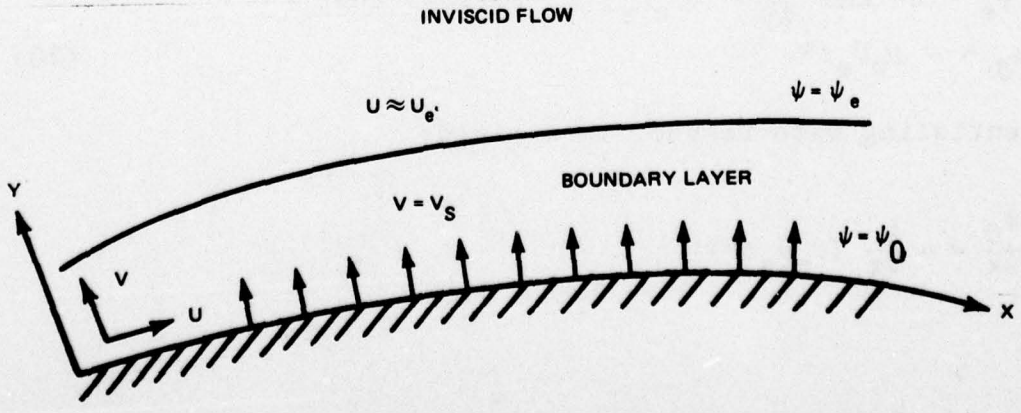

Fig. 4 Formulation of the Boundary Condition by the Surface Source Distribution

The iteration process begins with the computation of the inviscid flow over the airfoil systems. The first calculation of the displacement thickness is done using this inviscid flow. Successive computations are made using the inviscid flow over the equivalent bodies, these being obtained using nonzero Neumann boundary conditions at the body surfaces. Computations are done iteratively until compatibility between inviscid flow and displacement thickness is obtained, usually three or four iterations.

Occasionally in the first computation of the inviscid flow, velocities larger than the limiting velocity are generated near the leading edge of the slat. To give the iteration cycle a chance to make an initial correction to the circulation and thus cut down on these expansions, a lower limit on the speed of sound is set. This allows the relaxation to proceed with finite velocities everywhere. Also, after the source distribution is added on the surface some "wiggles" may develop in the potential flow solution near the trailing edge; these are caused by the large uncambering of the airfoil in the region and its large associated source distribution which suddenly ends at the trailing edge. Such irregularities in the pressure distribution would cause similar "wiggles" in the subsequent boundary layer computation and one could not expect the iteration process to converge under these conditions. Therefore the pressures near a trailing edge are extrapolated from a short distance upstream.

Separation is unfortunately a common phenomenon with high-lift configurations, and even more so at transonic speeds. Presently no attempt is made to model regions of separation that do not envelope the trailing edge; such separation regions usually occur on the concave lower surface of a slat. If the flow should separate before the trailing edge is reached and the separation region passes over it, an attempt to model the streamline passing over the separation region is made since the direction of the flow near the trailing edge is critical to the determination of the circulation. An empirical formula relating

the height between the trailing edge and the "inviscid" streamline to the free stream conditions on local geometry is utilized and a linearly growing source distribution that will generate this height is constructed.

5. RESULTS AND DISCUSSION

The method has been applied to a variety of two-element airfoil configurations and a few typical results are presented here. In order to evaluate the performance of the method independent of the particular strong interaction models and possible wind tunnel blockage corrections, an essentially incompressible case is considered first. Figure 5 shows the computed and measured (Ref. 27) surface pressure distributions on a NACA 23012 airfoil with a 2H flap. The plot depicts two inviscid calculations, the viscous interaction calculation and the wind tunnel data. The computed boundary layer growth on the main airfoil surface is small. On the flap upper surface, a separated flow region occurs which has a large effect on the lift. The agreement with experimental data is excellent except in the vicinity of the leading edge of the flap. The discrepancies in this region are due to slight differences between the goemetry of the configuration tested and that modeled by the computation. The wind tunnel model has a long lip extending from the trailing edge of the main airfoil. This protruberance, whose length is about 5% of the chord, was used to seal off the slot when the flap was retracted and reached over the leading edge of the flap, when it was extended. The conformal mapping method used in the computation cannot handle this geometric complexity. However, the modeled geometry, as shown in Fig. 5 seemed to produce quite acceptable results over most of the configuration.

Little transonic data on airfoils with leading edge slats is available and, like the previous case, these configurations have regions of separated flow. In Fig. 6, the computed pressure distribution and the experimental data (Ref. 28) for a NACA 64A010 airfoil with a slat at $M_\infty = 0.7$, $\alpha = 6^o$ and Re = 7.8 million are compared. Lower surface separation on the slat alters drastically the flow through the slot and again, substantial discrepancies occur near the leading edge of the downstream element (for this case the main airfoil). The method predicted

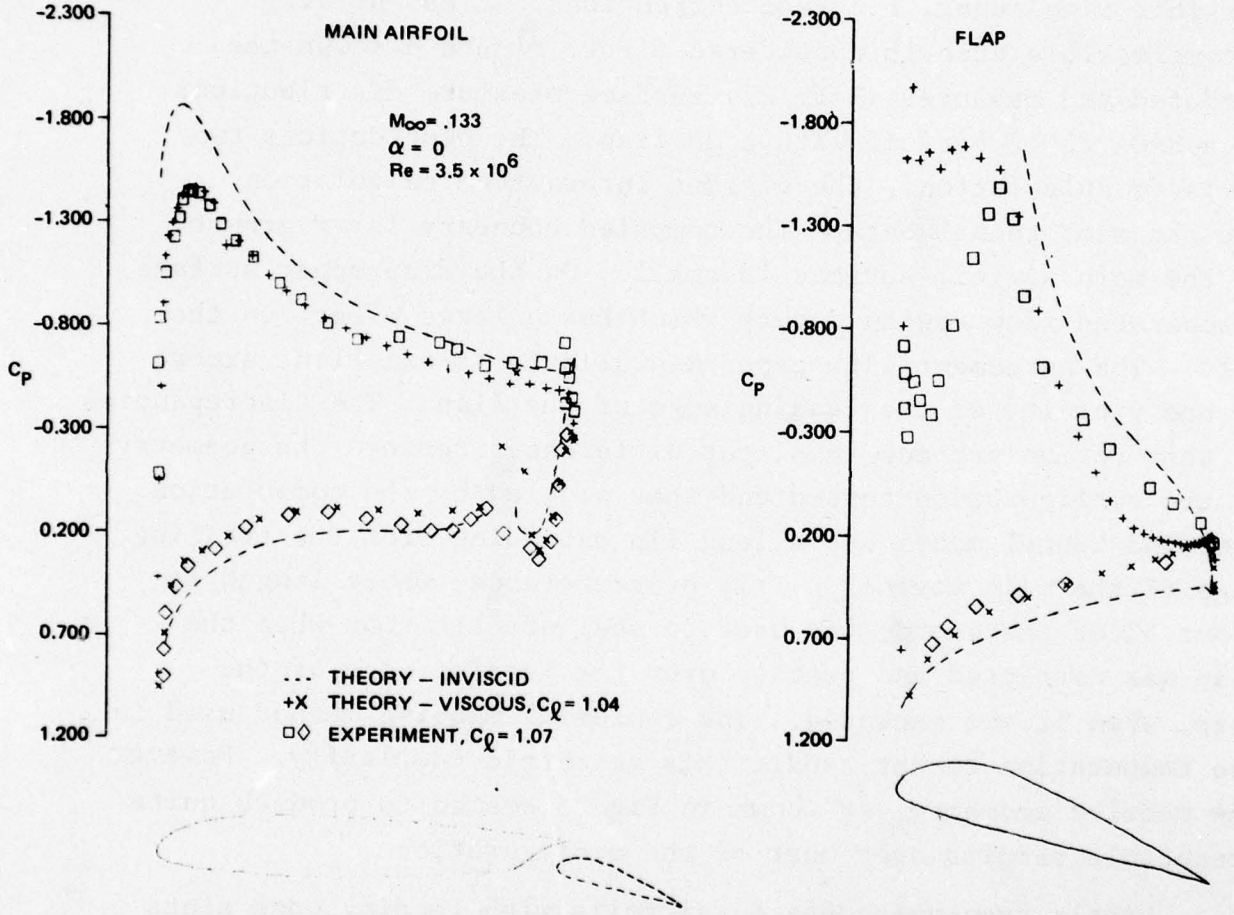

Fig. 5 Computed and Experimental Surface Pressure Distribution on an NACA 23012 Airfoil with 2H Flap Deflected 20°

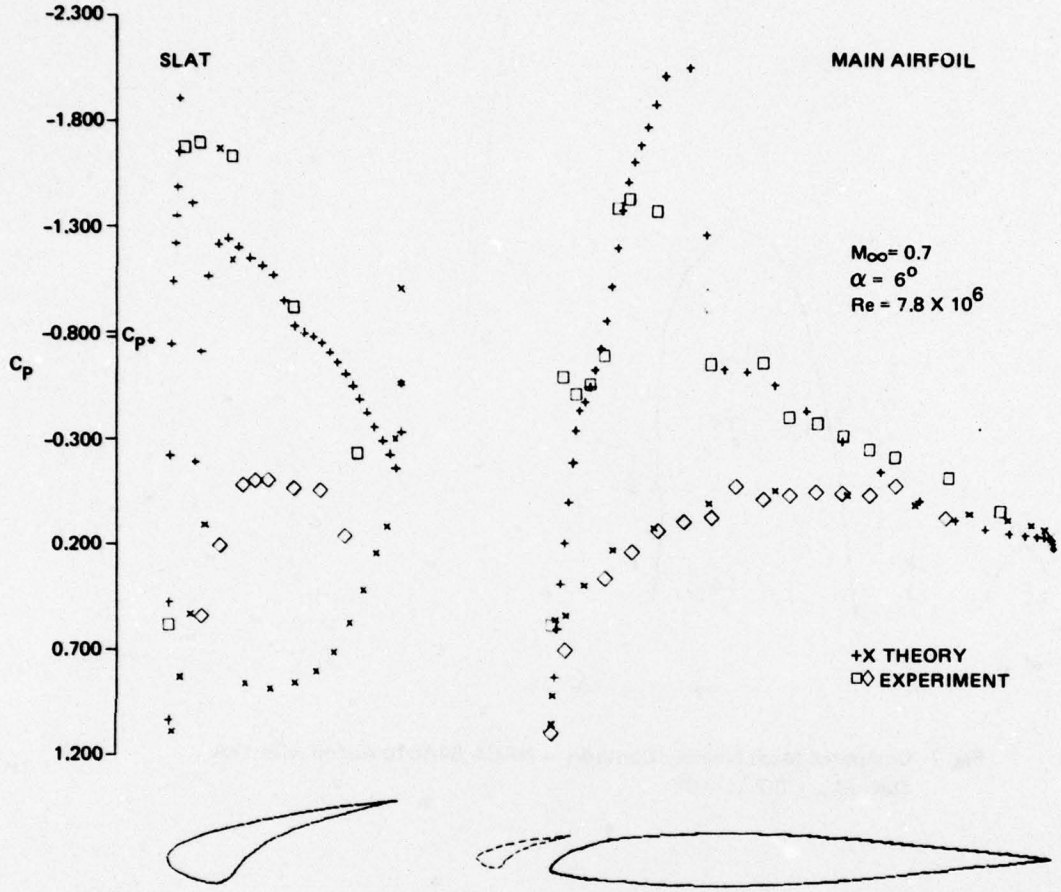

Fig. 6 Computed and Experimental Surface Pressure Distribution on an NACA 64A010 Airfoil with 18A Slat – $M_\infty = 0.7, \alpha = 6^o$

separation near the lower corner of the slat (which has been rounded slightly) but no attempt was made to model the massive separation region on the concave surface of the slat. Separation was also predicted on the upper surface of the slat, near the leading edge. On the main airfoil, away from the leading edge (slot) region satisfactory agreement with the data is obtained. Computed constant Mach number lines are shown in Fig. 7, indicating the imbedded regions of supersonic flow.

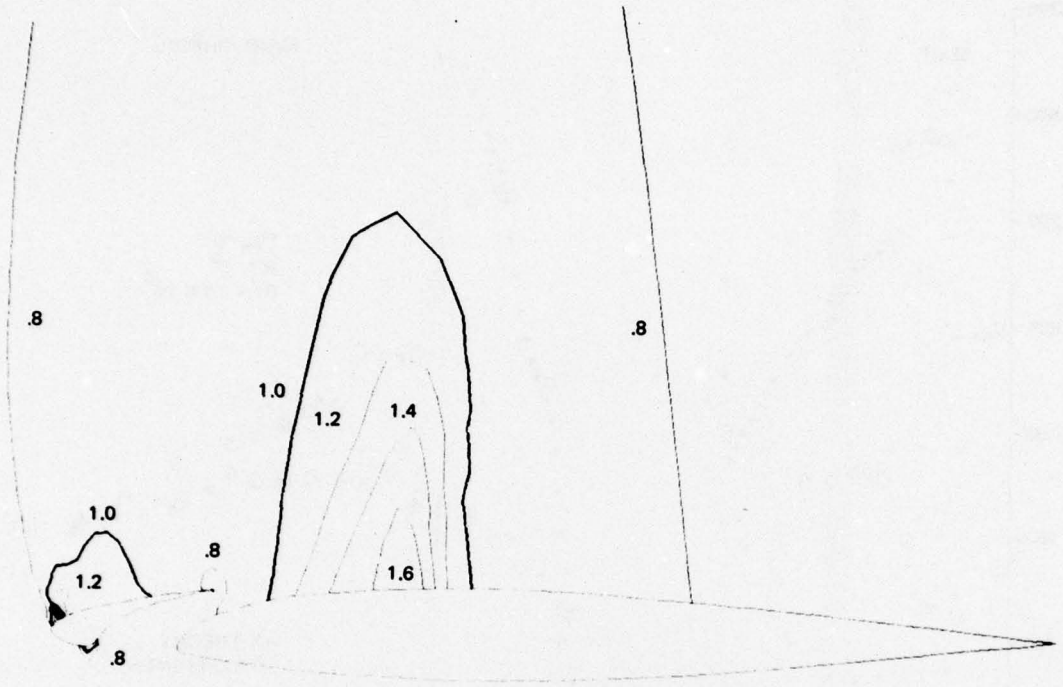

Fig. 7 Computed Mach Number Contours – NACA 64A010 Airfoil with 18A Slat - $M_\infty = 0.7, \alpha = 6^o$

The agreement is improved when the slat is more slender as in the configuration shown in Fig. 8. The arrangement was obtained from a basic NACA 64A406 airfoil (Ref. 1). The flow separation on the slat does not affect the flow coming out of the slot as much as it did in the previous case. The pressure distribution on the main airfoil is predicted quite well including the multiple peaks near the leading edge. Figure 9 shows the Mach number contours for this case. It is interesting to note the pocket of supersonic flow existing in the slot. The exit of the slot is essentially sonic with the flow quickly reaccelerating to supersonic velocities behind it. This pattern is reflected in the multiple peaks in both the computed and experimental pressures.

Figures 10 and 11 give results for two different positions of the slat. Both are high angle of attack cases and stall

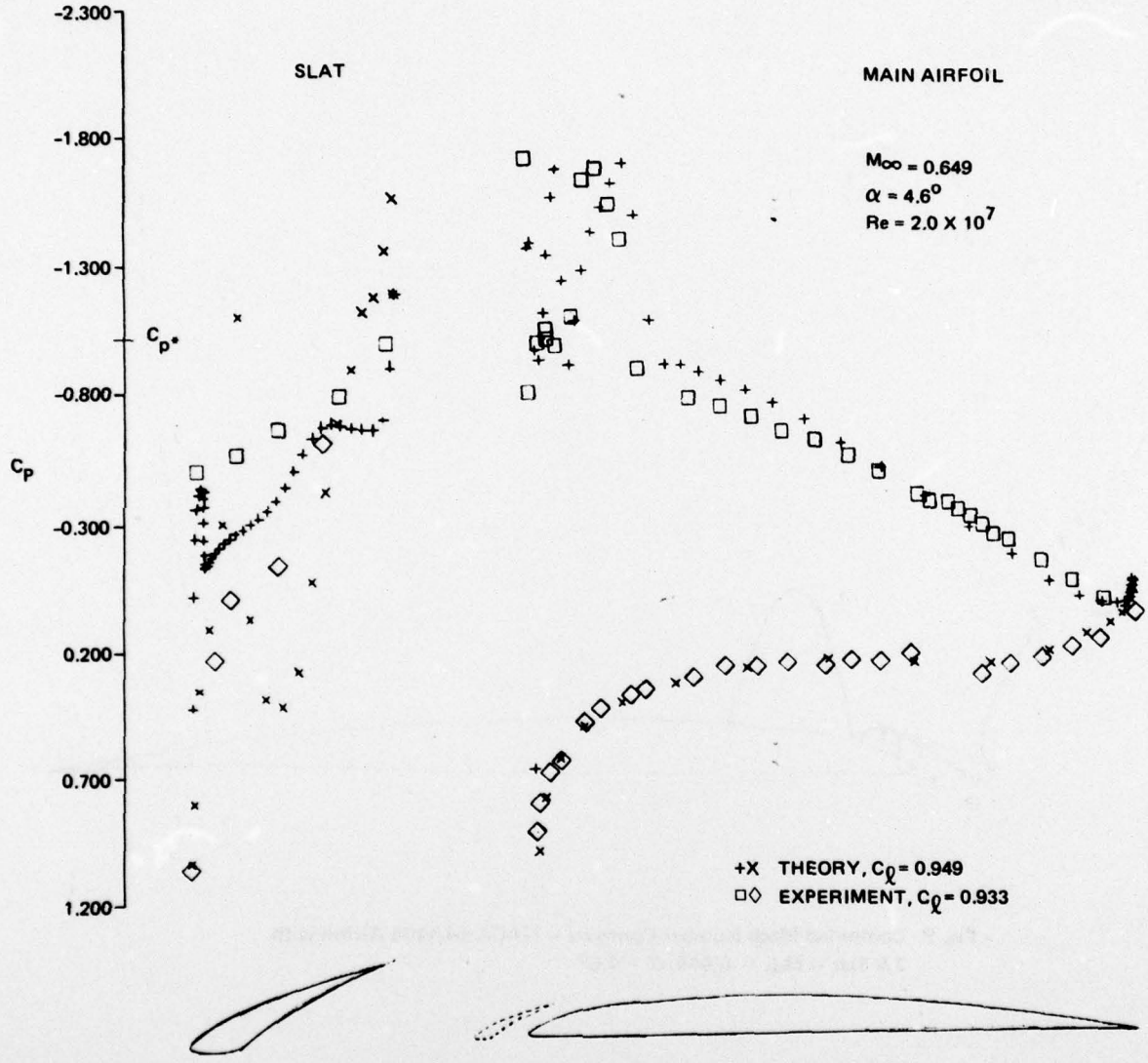

Fig. 8 Computed and Experimental Surface Pressure Distribution on an NACA 64A406 Airfoil with 7.8A Slat - $M_\infty = 0.649$, $\alpha = 4.6^o$

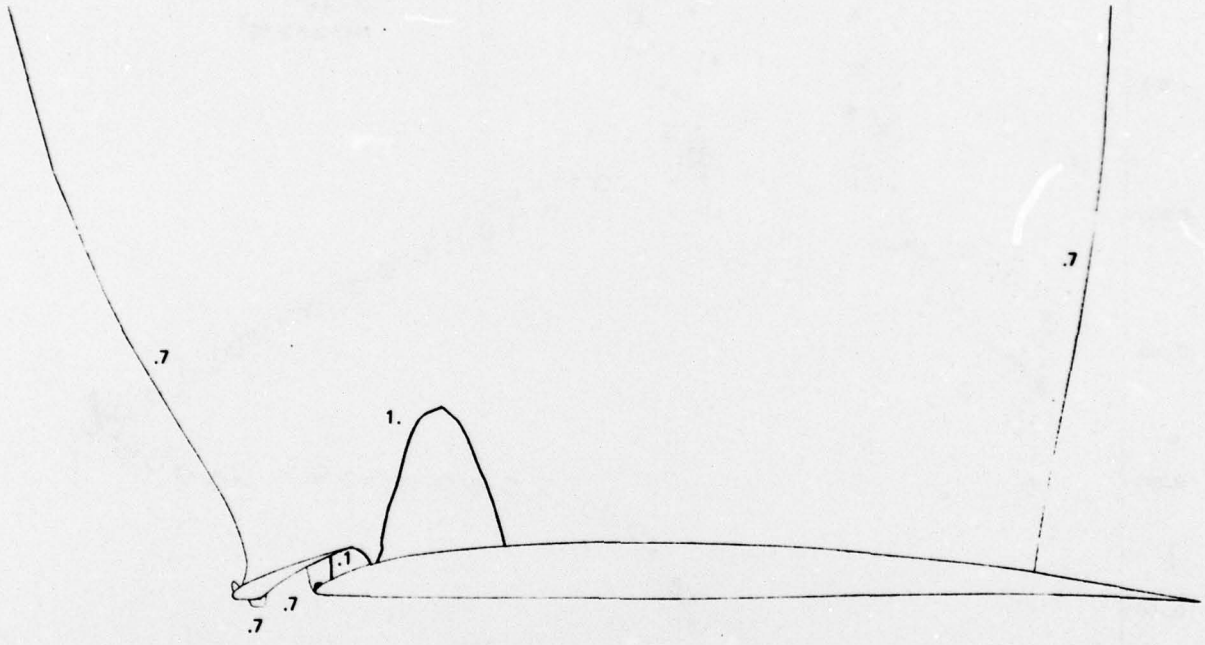

Fig. 9 Computed Mach Number Contours – NACA 64A406 Airfoil with 7.8 Slat – M_∞ = 0.649, α = 4.6°

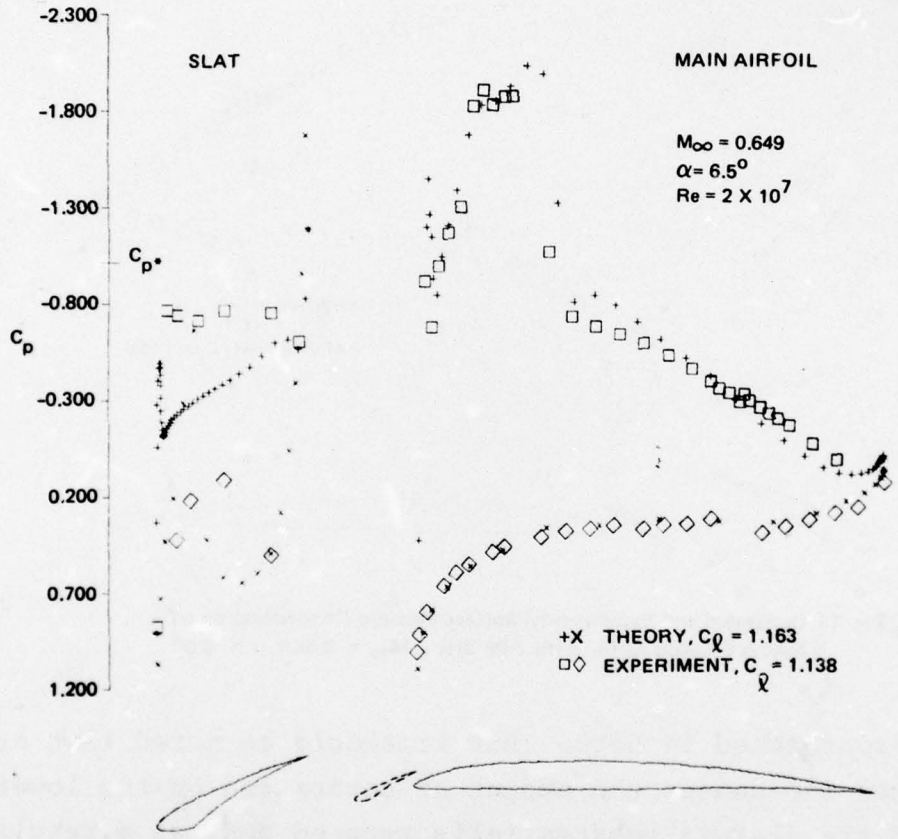

Fig. 10 Computed and Experimental Surface Pressure Distribution on an NACA 64A406 Airfoil with 10.6C Slat – M_∞ = 0.649, α = 6.5°

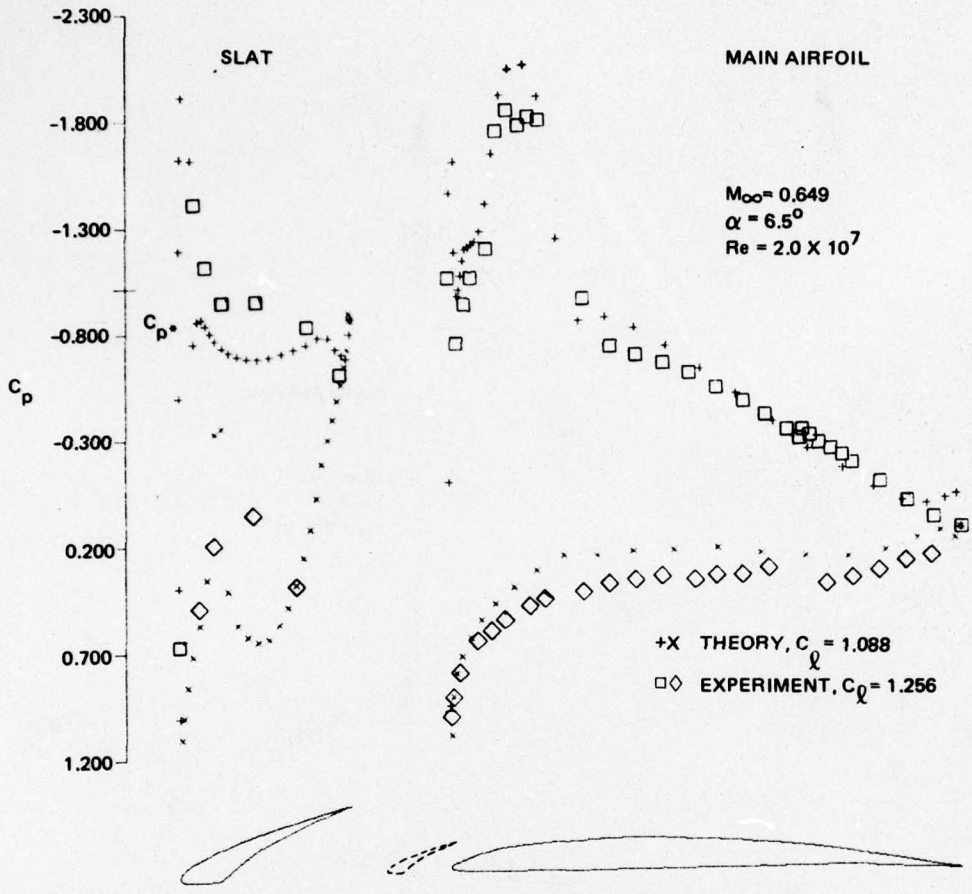

Fig. 11 Computed and Experimental Surface Pressure Distribution on an NACA 64A406 Airfoil with 7.8F Slat – M_∞ = 0.649, α = 6.5°

was being approached in both. But it should be noted that at these higher incidences the amount of separation on the lower surface of the slat is substantially reduced and, as a result, the agreement between data and computation is considerably improved in this region.

All the calculations were done at the Mach number and angle of attack quoted for the data. Thus the possible influence of wind tunnel blockage and flow angularities was not taken into account. Not unexpectedly, the comparisons with data have been marred by the presence of substantial regions of separation. But the reason for undertaking this study was

to develop a method that would help in the design of transonic maneuvering devices, and hopefully a good design would eliminate or at least minimize, the extent of flow separation. The present method can be used to infer the degradation in performance which they cause.

The numerical method, as has been shown, can handle an arbitrary two-element airfoil configuration. The computed results presented here were obtained on a series of two grid distributions, with a fine mesh of 60 points in the circumferential direction by 30 in the radial in the mapped domain. A typical supercritical case requires about 10 minutes of computing time on a IBM 370/168 computer. The computer code is far from being optimized and computational efficiency can be improved. Preliminary computations with the eigenvalue extrapolation procedure of Ref. 8 has indicated that a possible reduction of 40% can be obtained in the number of relaxation cycles needed to achieve a converged relaxation solution for the inviscid flow. This computation is by far the most time consuming portion of the method. The present semi-empirical model for the trailing edge interaction region although adequate, will soon be replaced by the more rational approach proposed by Melnik, Chow and Mead (Ref. 12). In addition the ability of the program to predict the forces should be assessed in order to determine whether the inviscid flow should be reformulated in conservation form.

6. REFERENCES

1 Caughey, D., "An Inviscid Analysis of Transonic, Slatted Airfoils," AIAA Journal of Aircraft, Vol. 13, 1976.

2. Murman, E.M. and Cole, J.D., "Calculation of Plane Steady Transonic Flows," AIAA J., Vol. 9, 1971.

3. Jameson, A., "Transonic Flow Calculations for Airfoils and Bodies of Revolution," Grumman Aerospace Corporation, Aerodynamics Report 390-71-1, 1971.

4. Garabedian, P.R. and Korn, D.G., "Analysis of Transonic Airfoils," Comm. Pure Appl. Math., Vol. 24, 1971.

5. South, F.C. Jr. and Jameson, A., "Relaxation Solutions for Inviscid Axisymmetric Transonic Flows over Blunt or Pointed Bodies," Proceedings of the AIAA Computational Fluid Dynamics Conference, pp. 8-17, 1973.

6. Grossman, B. and Melnik, R.E., "The Numerical Computation of the Transonic Flow over Afterbodies Including the Effect of Jet-Plume and Viscous Interactions," AIAA Paper 76-100, 1976.

7. Arlinger, B.G., "Calculation of Transonic Flow around Axisymmetric Inlets," AIAA Paper 75-80, 1975.

8. Caughey, D.A. and Jameson, A., "Accelerated Iterative Calculation of Transonic Nacelle Flow Fields," AIAA Paper 76-100, 1976.

9. Grossman, B. and Melnik, R.E., "The Numerical Computation of the Transonic Flow Over Two-Element Airfoil Systems," Proceedings of the Fifth International Conf. on Numerical Methods in Fluid Dynamics, Springer-Verlag, pp. 220-337, June 1976.

10. Grossman, B. and Volpe, G., "An Analysis of the Inviscid Transonic Flow Over Two-Element Airfoil Systems," Office of Naval Research Rept. ONR-CR215-241-1, June 1977.

11. Arlinger, B.G., "Analysis of Two Element High Lift Systems in Transonic Flow," ICAS Paper 1976.

12. Melnik, R.E., Chow, R., and Mead, H.R., "Theory of Viscous Transonic Flow Over Airfoils at High Reynolds Number," AIAA Paper 77-680, June 1977.

13. Ives, D.C., "A Modern Look at Conformal Mapping, Including Doubly Connected Regions," AIAA Paper 75-842, 1975.

14. Ludford, G.S.S., "The Behavior at Infinity of the Potential Function of a Two Dimensional Subsonic Compressible Flow," J. Math. Phys., Vol. 30, 1951.

15. Lagally, M., "Die Reibungslose Stromung in Aussengebiete Zwier Kreise, " ZAMM, Vol. 9, No. 4, pp. 209-305, Translated in NACA 626, 1929.

16. Jameson, A., "Iterative Solution of Transonic Flow Over Airfoils and Wings, Including Flows out Mach 1," Comm. Pure and Appl. Math., Vol. 27, 1974.

17. Thwaites, B., "Approximate Calculation of the Laminar Boundary Layer," Aeron. Quart., Vol. 1, 1974.

18. Rott, N. and Crabtree, L.F., "Simplified Laminar Boundary-Layer Calculations for Bodies of Revolution and for Yawed Wings," J. Aeron. Sci., August 1952.

19. Crabtree, L.F., "Prediction of Transition in the Boundary Layer," Aeron. Quart., Vol. 1, 1969.

20. Bradshaw, P., Ferriss, D.M., and Atwell, N.P., "Calculation of Boundary-Layer Development Using the Turbulent Energy Equation," J. Royal Aeron. Soc., Vol. 28, Part 3, 1967.

21. Green, J.E., Weeks, D.J., and Broomen, J.W.F., "Prediction of Turbulent Boundary Layer and Wakes in Compressible Flow by a Lag-Entrainment Method," RAE Technical Report 72231, 1973.

22. Lighthill, M.J., "On Displacement Thickness,"J. Fluid Mech., Vol. 4, 1958.

23. Volpe, G., "Recent Advances in Airfoil Analysis and Design," Grumman Aerodynamics Memorandum 75-27, 1975.

24. Volpe, G., "A Computer Program for Calculating Viscous Transonic Flows," Grumman Aerodynamics Memorandum 73-19, August 1973.

25. Bauer, F., Garabedian, P., Korn, D. and Jameson, A., Supercritical Wing Sections II, Springer-Verlag, N.Y., 1975.

26. Bavitz, P.C., "An Analysis Method for Two-Dimensional Transonic Viscous Flow," NASA TN D-7718, 1975.

27. Wenzinger, D.J. and Delano, J., "Pressure Distribution Over an NACA 23012 Airfoil with a Slotted and Plain Flap," NACA Report 633, 1938.

28. Axelson, J.A. and Stevens, G.L., "Investigation of a Slat in Several Different Positions on an NACA 64A010 Airfoil for a Wide Range of Subsonic Mach Numbers," NACA TN3129, 1954.

APPENDIX

CIRCUMFERENTIAL STRETCHING

An alternate circumferential stretching has been developed recently. In Ref. 10 it was reported that a suitable grid could be generated with the stretching

$$\theta = c_1 \sin \phi + c_2 \sin 2\phi + c_3 \qquad \text{(A-1)}$$

where ϕ is the azimuthal location of a point in the unstretched plane and θ is the stretched coordinate, c_1, c_2, and c_3 are three constants to be chosen by the user for each configuration. The proper concentration of grid points near the leading and trailing edges can be obtained also by having the azimuthal location of the same determined by the intersection of the ring $r = 1$ with radial lines emanating from the point of infinity at equal increments as shown in Fig. A-1. In the notation of Fig. A-1, these points can be located by

$$\cos \theta = r_\infty \sin^2\phi + \sqrt{1 + r_\infty^2 \sin^2\phi} \cos \phi \qquad \text{(A-2)}$$

This stretching does not require any inputs from the user. In the generation of the grid ϕ would be chosen at equal increments. This stretching is a natural development of the mapping which transformed infinity to a single off-center point. For the case where r_s and r_∞ go to zero θ and ϕ become identical. If the point of infinity were to be moved away from the center of the outer circle the same mapping would pull points on the unit circle around the circumference. The stretching given by Eq. (A-2) tends to reflect this phenomenon. An additional stretching which locates the point of infinity and each trailing edge exactly on grid lines is still used and has been described in Ref. 10.

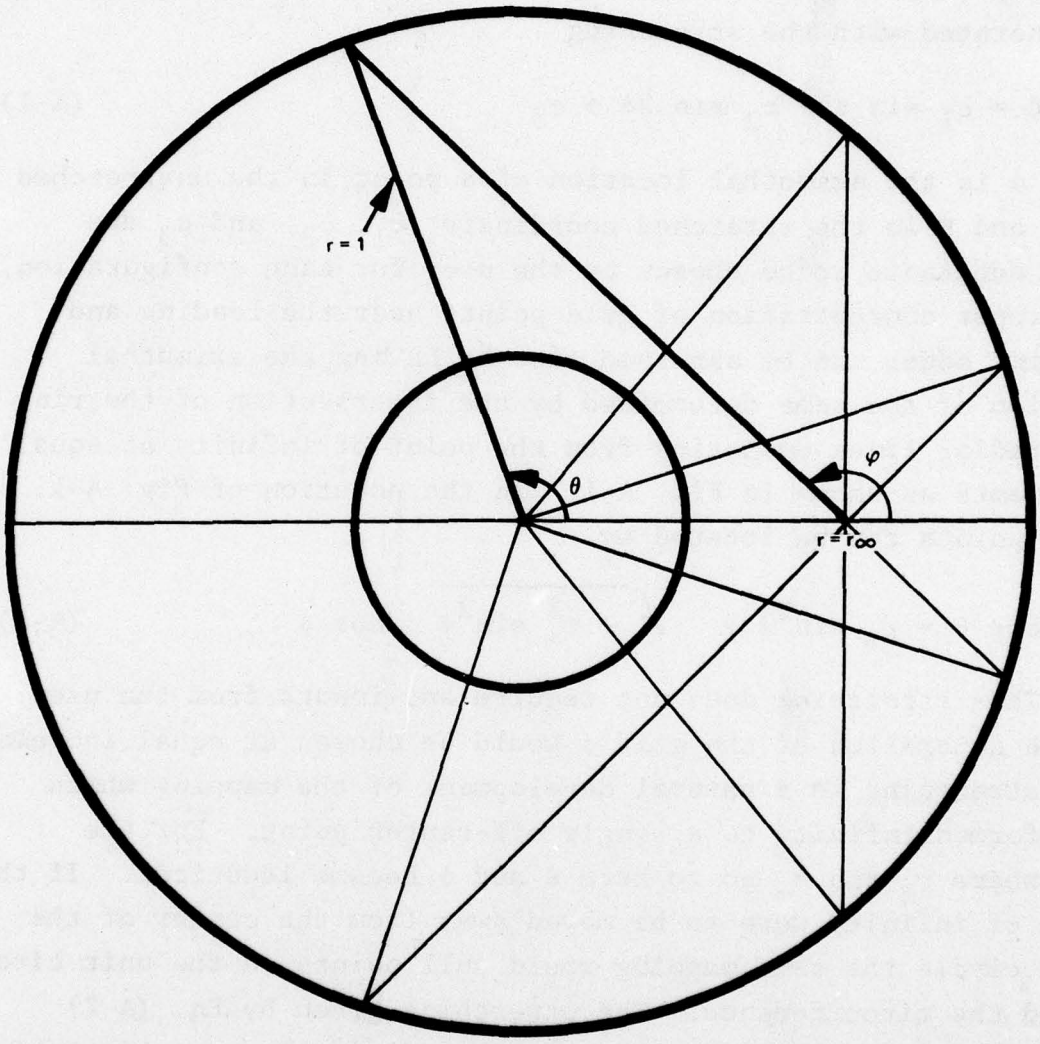

Fig. A-1 Circumferential Stretching

DISTRIBUTION LIST

Chief of Naval Research
Department of the Navy
Arlington, VA 22217
ATTN: Vehicle Technology Program
Code 211 5
Code 430B 1

Chief of Naval Development
Department of the Navy
Washington, DC 20360
ATTN: NAVMAT 0331 1
NAVMAT 0334 1

Naval Air Systems Command
Department of the Navy
Washington, DC 20351
ATTN: NAVAIR 320D 1
NAVAIR 5301 1
NAVAIR 53013 1

David Taylor Naval Ship Research
& Development Center
Bethesda, MD 20084
ATTN: Code 16 1
Code 522.3 1
Code 522.1 1

Naval Research Laboratory
Washington, DC 20375
ATTN: Technical Information
Office, Code 2627 1
Library, Code 2629 1

Superintendent
U. S. Naval Academy
Annapolis, MD 21402 1

Superintendent
U. S. Naval Postgraduate School
Monterey, CA 93940 1

U. S. Naval Air Development Center
Warminster, PA 18974
Air Vehicle Technology Dept.
ATTN: Code 301 1

ONR Branch Office
1030 East Green Street
Pasadena, CA 91106
ATTN: Mr. B. F. Cagle 1

ONR Branch Office
495 Summer Street
Boston, MA 02210
ATTN: Dr. A. D. Wood 1

ONR Branch Office
536 South Clark Street
Chicago, IL 60605
ATTN: Mr. M. A. Chaszeyka 1

Commandant of the Marine Corps
Washington, DC 20380
ATTN: Dr. A. L. Slafkosky
Scientific Advisor
(Code RD-1) 1

Defense Documentation Center
Cameron Station, Bldg. 5
Alexandria, VA 22314 12

Department of the Army
DCS for Research and Development and
Acquisition
Washington, DC 20310
ATTN: DAMA-WSA (Mr. R. L. Ballard) 1

U. S. Army Material Command
5001 Eisenhower Avenue
Alexandria, VA 22333
ATTN: AMCRD-F 1

Director, Headquarters
U. S. Army Air Mobility R&D Lab.
Ames Research Center
Moffett Field, CA 94035 1

Director, Ames Directorate
U. S. Army Air Mobility R&D Lab.
Ames Research Center
Moffett Field, CA 94035 1

Director, Langley Directorate
U. S. Army Air Mobility R&D Lab.
Langley Research Center
Hampton, VA 23665 1

Director, Eustis Directorate
U. S. Army Air Mobility R&D Lab.
Fort Eustis, VA 23604 1

U. S. Air Force Flight Dynamics Laboratory
Wright-Patterson AFB, OH 45433
ATTN: PT, Prototype Division 1
FXM, Aeromechanics Branch 1

Air Force Office of Scientific Research
Directorate of Aerospace Sciences
Bolling AFB, DC 20332 1

National Aeronautics and Space Administration
600 Independence Avenue, SW
Washington, DC 20546
ATTN: Code RAA 1
Code RAV 1

National Aeronautics and Space Administration
Ames Research Center
Moffett Field, CA 94035
ATTN: Dr. T. Gregory, Code FAE 1
Dr. G. Chapman, Code FAR 1

National Aerodynamics and Space Administration
Langley Research Center
Hampton, VA 23665
Subsonic, Transonic Aerodynamic Div.
ATTN: Dr. James F. Campbell 1
Dr. Stephen Wornom 1

Flow Research, Inc.
1819 South Central Avenue
Kent, WA 98031
ATTN: Dr. E. Murman 1

Lockheed Missiles & Space Co., Inc.
Huntsville Research & Engineering Center
P. O. Box 1103
Huntsville, AL 35807
ATTN: Mr. A. Zalay 1

Rockwell International
Science Center
Thousand Oaks, CA 91360
ATTN: Dr. N. Malmuth 1

Nielsen Engineering & Research, Inc.
510 Clyde Avenue
Mountain View, CA 94043 1

University of Cincinnati
Department of Aerospace Engineering and Applied Mechanics
Cincinnati, OH 45221
ATTN: Dr. R. T. Davis 1

New York University
Courant Institute of Mathmatical Sciences
New York, NY 12203
ATTN: Dr. A. Jameson 1

Dynamics Technology Inc.
3838 Carson Street
Suite 110
Torrance, CA 90503 1

McDonnell Douglas Aircraft Co.
P. O. Box 516
St. Louis, MO 63166
ATTN: Dept. 241, R. B. Jenny 1
Dept 230, R. W. McDonald 1